The Role of Convective Outflow in the Waldo Canyon Fire*

RICHARD H. JOHNSON, RUSS S. SCHUMACHER, AND JAMES H. RUPPERT JR.

Colorado State University, Fort Collins, Colorado

DANIEL T. LINDSEY

NOAA/Center for Satellite Applications and Research, and Cooperative Institute for Research in the Atmosphere, Colorado State University, Fort Collins, Colorado

JULIA E. RUTHFORD

NOAA/National Weather Service, Charleston, West Virginia

LISA KRIEDERMAN

NOAA/National Weather Service, Denver/Boulder, Colorado

(Manuscript received 13 November 2013, in final form 28 March 2014)

ABSTRACT

The meteorological conditions associated with the rapid intensification and spread of the catastrophic Waldo Canyon fire on 26 June 2012 are studied. The fire caused two fatalities, destroyed 347 homes in Colorado Springs, and resulted in insurance losses of nearly $0.5 billion (U.S. dollars), making it the most economically destructive fire in Colorado's history. While the fire was first discovered on 23 June, the paper focuses on 26 June, when it grew explosively and rapidly advanced eastward into a heavily populated area on the west side of Colorado Springs. Near-record hot and dry conditions prevailed over the Intermountain West prior to the fire, along with a persistent upper-level ridge. On 26 June, a narrow tongue of moist air aloft originating over the Southwest shifted from Utah into Colorado. Dry conditions at low levels and moisture aloft set the stage for strong microburst-producing thunderstorms to develop over Colorado. Convective cells first formed at midday over the San Juan Mountains, later consolidating into a thunderstorm complex that produced an organized convective outflow with strong, gusty winds at the surface. The leading gust front associated with the outflow moved past the Waldo Canyon fire at the hottest time of the day with recorded wind gusts up to 26 m s^{-1}. The rapid eastward advance of the fire, as well as an onset of pyrocumulonimbus and lightning activity, was timed with the passage of the gust front. A numerical simulation, initiated one day earlier, produced mesoscale features closely resembling those observed, including the gust front passage at the fire and the vertical structure of the convective outflow.

1. Introduction

The U.S. fire season of 2012 was exceptionally destructive, with over nine million acres of land burned, the third greatest areal extent in the past 53 years (http://www.nifc.gov). Hot and dry conditions contributed to numerous fires throughout the Intermountain West, many of which occurred in Colorado. Among these, the Waldo Canyon fire near Colorado Springs, Colorado, proved to be the most economically destructive in Colorado's history. It resulted in two fatalities, destroyed 347 homes,[1] burned over 18 000 acres, and led to insurance

*Supplemental information related to this paper is available at the Journals Online website: http://dx.doi.org/10.1175/MWR-D-13-00361.s1.

Corresponding author address: Richard H. Johnson, Dept. of Atmospheric Science, Colorado State University, 200 West Lake Street, 1371 Campus Delivery, Fort Collins, CO 80523-1371.
E-mail: johnson@atmos.colostate.edu

DOI: 10.1175/MWR-D-13-00361.1

© 2014 American Meteorological Society

[1] In terms of homes lost, the Waldo Canyon fire has now been exceeded by the mid-June 2013 Black Forest fire northeast of Colorado Springs, where 511 homes were destroyed.

claims totaling $454 million (U.S. dollars; http://www.rmiia.org/catastrophes_and_statistics/Wildfire.asp). While the stage for the Waldo Canyon fire was set by a prolonged drought and excessive heat over the region, this study focuses on a shorter-term meteorological event, a convectively generated gust front and its impact on the advance and intensification of the fire on 26 June, which ultimately contributed substantially to the above losses.

On the afternoon of 26 June, the Waldo Canyon fire surged eastward, descending out of the foothills into housing developments on the west side of Colorado Springs. In a matter of hours, hundreds of homes were enveloped by the fire, aided by embers blown out ahead by strong westerly winds. The fire had undergone substantial growth for several preceding days, but its expansion and eastward movement on 26 June were dramatic (Ruthford and Kriederman 2013). The fire area more than tripled in size from 25 to 26 June and total evacuees grew from ~2000 to nearly 30 000 on 26 June. Several studies (Ruthford and Kriederman 2013; Johnson et al. 2013; Meister 2013; Stark 2013) have reported preliminary findings related to the meteorological and operational aspects of the fire.

In this paper, an analysis of the meteorological conditions associated with Waldo Canyon fire on 26 June is presented. A strong thunderstorm gust front swept through Colorado Springs late in the afternoon on 26 June. The convective outflow, which had the characteristics of a macroburst (Fujita 1985), grew out of a thunderstorm complex that had its first origins over the mountains of southwest Colorado. This paper documents the synoptic-scale conditions that favored the formation of macroburst-type thunderstorms on that day, the development of incipient convection in southwestern Colorado, and the progression of the associated gust front through the Waldo Canyon fire area. The passage of the gust front was accompanied by strong westerly flow, which significantly impacted the behavior of the fire. In addition to the observational study, a numerical simulation has been carried out that reproduces the formation of macroburst-producing storms over the southwestern part of the state by midday on 26 June and the passage of an associated gust front through the fire later in the afternoon.

2. Background

a. Antecedent conditions

Anomalously warm and dry conditions prevailed throughout the Intermountain West in the months prior to the outbreak of the spring and summer wildland fires of 2012. The January–June 2012 period was the second driest and second warmest in Colorado in 118 years of records, while many other states in the region had similar

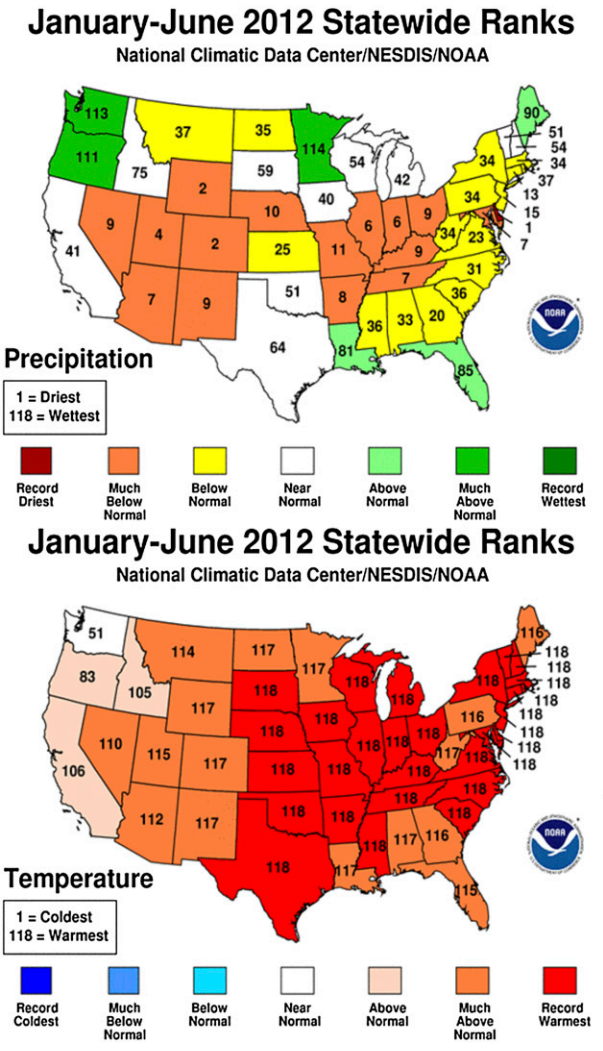

FIG. 1. January–June 2012 statewide average (top) precipitation and (bottom) temperature rankings. This period was the second driest and warmest in recorded Colorado history.

near-record conditions (Fig. 1). Below-average late-winter snowpacks were compounded by a very dry and warm spring such that spring and early summer runoff over most of the region was well below average, and in many Colorado River basins worse than 2002 or other benchmark dry years for the region (1977, 1992) (http://wwa.colorado.edu). This situation led to very dry fuel conditions throughout the state. The Energy Release Component (ERC; a National Fire Danger Rating System index that indicates how hot a fire can burn) was at a 19-yr high level for the Central Front Range of Colorado during a two-week period centered around the time of the fire (http://gacc.nifc.gov/rmcc/). By a substantial margin, the year 2012 broke the previously held March–April–May mean temperature record for the United States that occurred in 1910, the year of "The Big Burn"

FIG. 2. Map of Waldo Canyon fire perimeter superimposed on terrain to the west of Colorado Springs. Fire started on 23 Jun 2012 in enclosed blue area. Times of fire perimeters correspond approximately to midnight at the beginning of the dates indicated. Also indicated are locations of geographic features referred to in the text, as well as the Air Force Academy High Wind Alert Station (HWAS) on Rampart Ridge. [Map courtesy of NOAA/National Weather Service (NWS), Pueblo, Colorado.]

forest fire in northeast Washington, northern Idaho, and western Montana (Diaz and Swetnam 2013).

b. *Timeline of fire*

The fire was first discovered along a trail area within the Waldo Canyon early on 23 June (Fig. 2).[2] Rather significant growth ensued, with the fire covering an area of 2500 acres (1012 ha) by the end of the day. The fire continued to expand on 24 June reaching a size of 3600 acres (1457 ha). On 25 June, brisk south-southeasterly flow pushed the fire northward in a narrow stretch along Rampart Range (Fig. 2), which set the stage for a broad eastward advance the following day. By the end of 25 June, the fire had grown to 4500 acres (1821 ha), but then more than tripled in size on 26 June, eventually covering 15 622 acres (6322 ha). A major portion of the advance on 26 June was eastward down the east slopes of the Rampart Range into the western part of Colorado Springs (Fig. 2).

As a guide to interpreting the relationship between meteorology and the progression of the fire on 26 June, a timeline of various events (fire behavior, weather conditions, operational actions, etc.) is presented in Table 1. Information sources for the events include the City of Colorado Springs Final After Action Report (hereafter AAR; https://www.springsgov.com), the incident meteorologists (IMETs) assigned to the fire,[3] and other sources as indicated.

The synoptic-scale conditions over the western United States on the days preceding 26 June are reviewed in section 4. The National Weather Service Weather Forecast Office Pueblo, which provided forecasting support for the fire, anticipated changing conditions to develop in the fire area, issuing a red flag warning in the afternoon of 25 June indicating that a combination of strong winds from thunderstorms, low relative humidity, and high temperatures posed a threat of explosive fire growth potential later on 26 June. On the morning of 26 June, indications of an active fire day

[2] As of this writing, the cause of the fire has not yet been determined.

[3] Coauthors Lisa Kriederman and Julia Ruthford.

TABLE 1. Timeline for Waldo Canyon fire on 26 Jun 2012. MDT* = UTC − 6 h, AAR = Colorado Springs Final After Action Report, and IMET = incident meteorologist.

Time (MDT*)	Event	Source
~0600	Downslope conditions overnight; poor morning relative humidity recovery; convective environment already present: altocumulus castellanus and early fire columns	IMET
Midmorning to mid- to late afternoon	South-to-southeasterly flow throughout period; deep convective boundary layer and extremely dry conditions; instability-driven fire growth regime; westward, northward, and eastward growth of fire perimeter (Figs. 2 and 12)	IMET, AAR
1339	Pre-evacuation orders given for Mountain Shadows (Fig. 2) and neighboring communities	AAR
1429	Report of fire on west side of Williams Canyon (Fig. 2)	AAR
~1430	Vigorous pyrocumulus observed	IMET, Fig. 3a
1509	Colorado Springs sets all-time record-high temperature: 101°F (38°C)	NWS
1545	Report of fire ~107 m from bottom of Queens Canyon	AAR
1608	Fire on east side of east-facing ridge of Queens Canyon	AAR
1620	Report that fire moved one-third of way down eastern ridge of Queens Canyon	AAR
1621	Mandatory evacuation ordered for Mountain Shadows area	AAR
1653	Arrival of thunderstorm gust front at mesonet station atop Rampart Ridge (Rampart HWAS, Fig. 2); strong west-southwest winds gusting to 26 m s^{-1} (59 mph) shortly after 1700 (Figs. 12 and 13a)	Air Force Academy mesonet
1707–1717	Strong westerly winds drive fire rapidly eastward and downhill into Mountain Shadows (Fig. 2)	AAR
1710	Onset of first lightning activity since start of fire	Lang et al. (2014)
1711	Collapse of fire column reported	AAR
1745	Onset of second, stronger burst of lightning activity	Lang et al. (2014)
1750	Vigorous pyrocumulonimbus coincident with strong lightning activity	Fig. 3b; Lang. et al.
1822–2146	Additional mandatory evacuation orders given for ~20 000 residents on west side of Colorado Springs	AAR
By end of day	Total evacuees grew to 28 770; fire area more than tripled in size, growing from 4500 to 15 622 acres	AAR

were already evident: very low relative humidities, the presence of altocumulus castellanus (Corfidi et al. 2008), and early fire columns (Table 1). Brisk south-to-southeasterly flow prevailed over the region from mid-morning to mid- to late afternoon. Aided by a deep convective boundary layer and extremely dry conditions, an instability-driven fire growth regime was well under way by midday. Around 1430 LT, pyrocumulus (Fromm et al. 2010) began to be observed (Fig. 3a). By mid-afternoon, Colorado Springs set an all-time record-high temperature of 38°C (101°F). During the period 1430–1600 LT, the fire began moving into Williams and

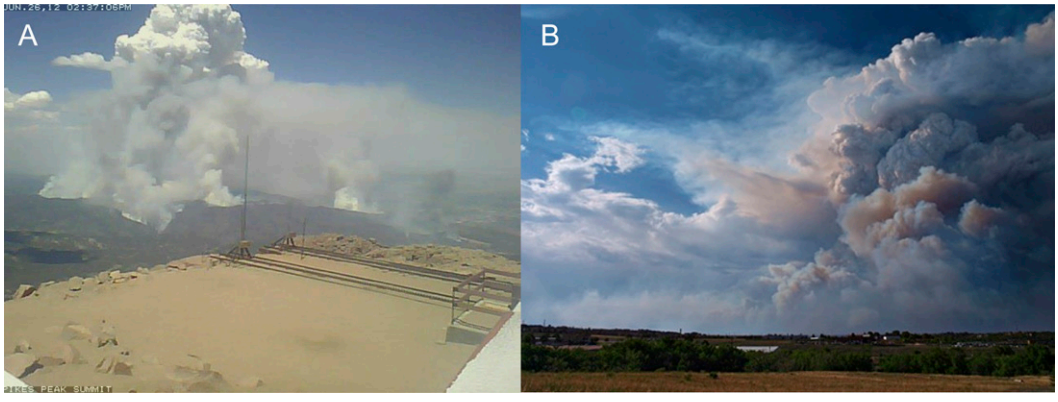

FIG. 3. (a) Waldo Canyon fire at 2037 UTC (1437 LT) 26 Jun 2012 from atop Pikes Peak (source: NWS Pueblo, Colorado) and (b) at 2350 UTC (1750 LT) from 8th Street in southwest Colorado Springs (source: E. Beute). Pyrocumulonimbus (with lightning activity) was evident at this time during the height of the fire.

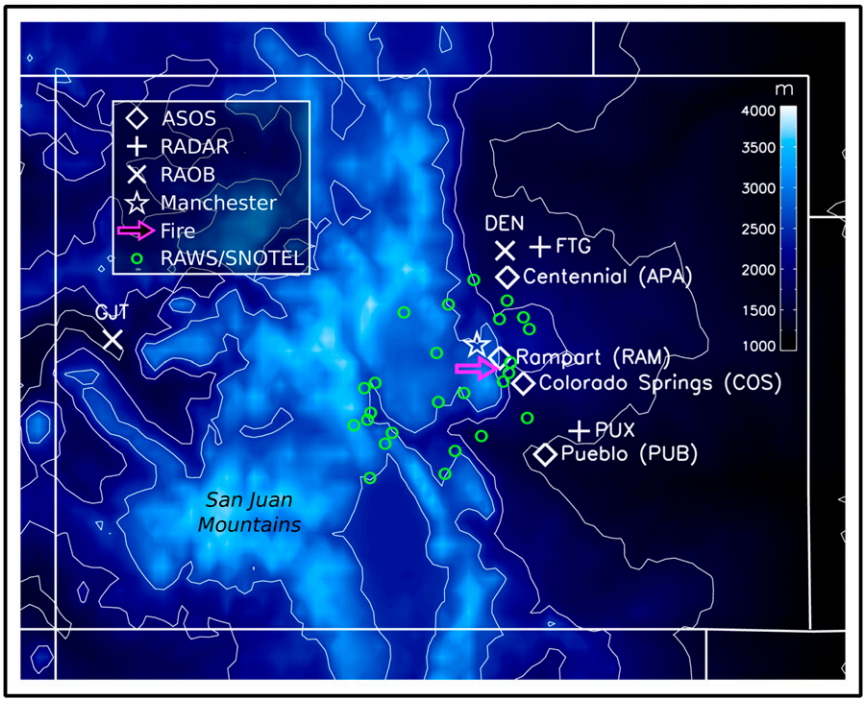

FIG. 4. NWS radar, ASOS, and sounding (raob) sites used in the analysis of convection and associated gust fronts over Colorado. Dots designate RAWS and SNOTEL sites used in the mesoanalyses, with the Manchester site denoted by a star. Meteograms in Fig. 13 are for sites indicated by diamonds. Fire location is at tip of arrow. Elevations are in m with thin lines at 500-m intervals. Location of San Juan Mountains, where convective outflow first formed (Fig. 11), is indicated.

Queens Canyons to the west of Colorado Springs (Fig. 2). By 1620 LT, there were reports that the fire had grown to such an extent that it had moved one-third of the way down the eastern ridge of Queens Canyon, placing it just west of the Mountain Shadows neighborhood, leading to mandatory evacuations of that community.

A significant change in the weather conditions occurred shortly thereafter as a thunderstorm gust front (to be discussed in detail later) arrived at the fire. Its passage at an Air Force Academy mesonet station atop Rampart Ridge (Rampart HWAS, Fig. 2) occurred at 1653 LT, with west-southwesterly winds gusting to 26 m s^{-1} shortly after 1700 LT. Between 1707 and 1717 LT, the Colorado Springs Fire Department reported strong westerly winds driving the fire rapidly eastward and downhill into the Mountain Shadows neighborhood (Fig. 2). At 1710 LT, the first lightning [all intracloud (IC)] associated with the fire was observed (Lang et al. 2014), followed by a second, stronger burst of IC lightning activity at 1745 LT when vigorous pyrocumulonimbus had developed (Fig. 3b). During the period 1822–2146 LT, additional evacuation orders were given for ~20 000 residents in the western neighborhoods of Colorado Springs.

c. *Factors in fire evolution on 26 June*

While an increase in the intensity and rate of eastward spread of the fire was timed with the passage of the gust front, it is important to note that other factors likely contributed to changes in the fire behavior on this day. Viegas and Simeoni (2011) emphasize the important roles of three factors—fuel bed properties, topography, and meteorological conditions—in the rate of spread of a fire. These factors can have varying degrees of influence that are often difficult to sort out. Moreover, changes in intensity and rate of spread can also arise from fire–atmosphere interactions generated by the fire itself (Potter 2012). All of these factors could have played a role in the intensification and rapid spread of the fire; however, it is beyond the scope of the paper to fully evaluate their individual contributions. The point we wish to emphasize is that meteorological conditions—the passage of a gust front and shift to strong westerly winds—were a factor reported by observers to have significantly impacted the fire, pushing it

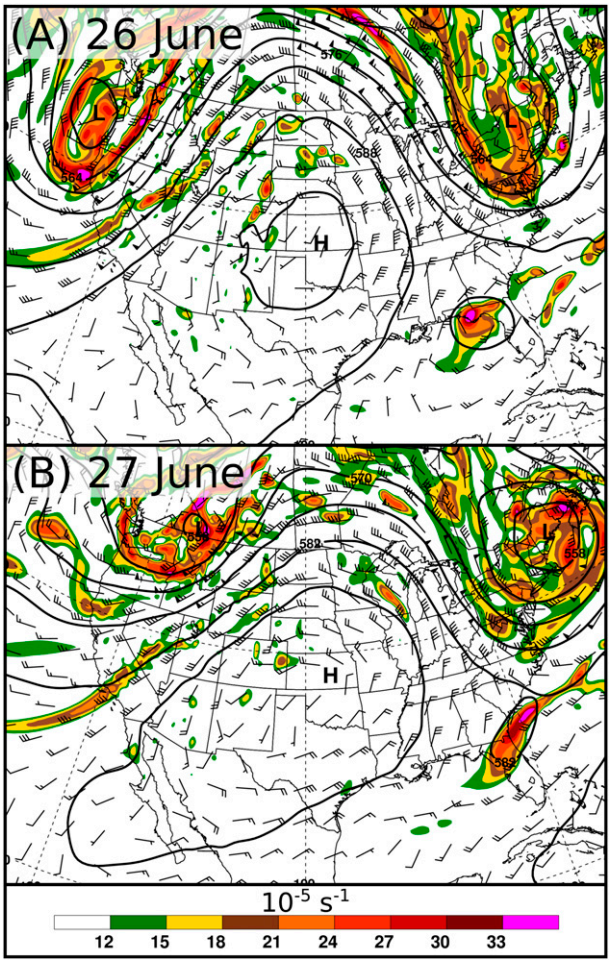

FIG. 5. Heights (contours, dam), absolute vorticity (shaded, $10^{-5}\,s^{-1}$), and winds (flag = $25\,m\,s^{-1}$, full barb = $5\,m\,s^{-1}$, and half barb = $2.5\,m\,s^{-1}$) at 500 hPa at 0000 UTC (a) 26 Jun and (b) 27 Jun 2012 based on GFS analysis.

downhill into the Mountain Shadows neighborhood late on 26 June.

d. *Meteorological phenomena impacting other recent fires*

Other instances of significant synoptic or mesoscale weather events related to fire behavior have recently been reported. Engel et al. (2013) investigated the impact of various synoptic- to mesoscale features on fire danger indices associated with the 7 February 2009 "Black Saturday" fires over the state of Victoria, Australia. They found that boundary layer horizontal convective rolls, unsteady gravity currents, and nocturnal bores modified the local environment contributing to large spatial and temporal variability in indices related to fire behavior. More recently, at the July 2013 Yarnell Hill fire in Arizona, 19 fatalities occurred coincident with the arrival of a gust front at the fire (https://docs.google.com/file/d/0B36DIycSgbzWSUtjNkl1Z2ROT0k/edit).

e. *Summary*

To summarize this section, the Waldo Canyon fire saw rather substantial growth for several days following first detection on 23 June, but its expansion on 26 June was dramatic. Record-setting heat and very dry conditions during the daytime contributed to an instability-driven growth regime through the midday period with an associated expansion of the fire area in nearly all directions. However, the fire exhibited significant changes in the afternoon with the arrival of a gust front in the region. The accompanying strong westerly winds drove the fire downhill into Colorado Springs neighborhoods, forcing extensive evacuations and destroying many homes. The first lightning associated with the fire was observed during this time as intense pyrocumulonimbus developed. By the end of the day, the total burn area had more than tripled in size.

3. Data and modeling procedures

a. *Data for synoptic-scale and mesoscale analyses*

A map of the various sites that collected data used in subsequent mesoanalyses is shown in Fig. 4. A mix of surface observations has been utilized: National Weather Surface (NWS) Automated Surface Observing System (ASOS) from the National Oceanic and Atmospheric Administration (NOAA) National Climatic Data Center (NCDC; http://www.ncdc.noaa.gov/), Remote Automated Weather System (RAWS), Snow Telemetry (SNOTEL) stations, and the Air Force Academy mesonet sites (http://hwas.usafa.edu/). RAWS and SNOTEL data have been obtained from the University of Utah MesoWest website (http://mesowest.utah.edu; Horel et al. 2002). Surface data from these networks are used to identify and track outflow boundaries from thunderstorms originating at midday over southwest Colorado. Surface mesoanalyses are complicated owing to the complex and mountainous terrain of the region, the irregular frequency and spacing of the surface observations, and the inconsistent data quality from the diverse platforms. Nevertheless, the ability to investigate mesoscale phenomena in the Intermountain West has been vastly improved over the past two decades by the advent of enhanced surface observations in support of fire weather operations, water resource management, and other applications (Myrick and Horel 2008; Steenburgh et al. 2009).

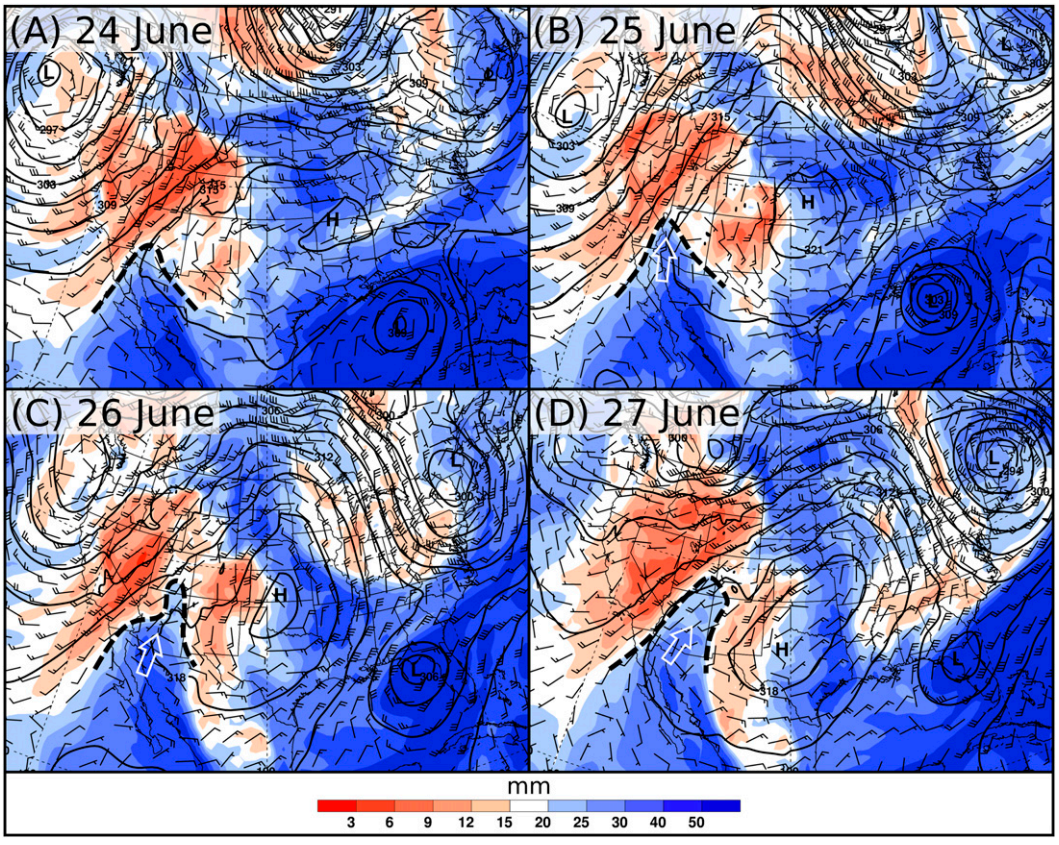

FIG. 6. 700-hPa heights (contours, dam), winds, and precipitable water (mm) at (a)–(d) 0000 UTC 24–27 Jun 2012. Dashed line shows approximate position of 20-mm contour. Arrow indicates direction of moisture transport.

Sounding data were obtained from the University of Wyoming (http://weather.uwyo.edu/upperair/sounding.html). Synoptic-scale analyses were prepared from the Global Forecast System (GFS) archive at the NOAA/National Operational Model Archive and Distribution System (NOMADS; http://nomads.ncdc.noaa.gov/).

b. Radar and satellite data

Level-II Weather Surveillance Radar-1988 Doppler (WDR-88D) reflectivity and velocity data from Pueblo (PUX) and Denver (FTG), Colorado (Fig. 4), are utilized to track the progression of gust fronts across the Colorado Springs area. To produce a large-scale mosaic of the radar reflectivity field for a set of mesoanalyses, base-scan reflectivity data (~0.5°) were collected for a given time from PUX and FTG, and the data points nearest to their parent station were plotted. This procedure exploits the lowest-elevation reflectivity data possible from the two stations. The Gibson Ridge GR2Analyst software package is employed to create vertical cross sections of the radar reflectivity and radial velocity fields from the PUX WSR-88D data as well as 3D displays (http://www.grlevelx.com/gr2analyst). Visible and infrared satellite data are obtained from *Geostationary Operational Environmental Satellite-15* (*GOES-15*) and water vapor data from *GOES-13*.

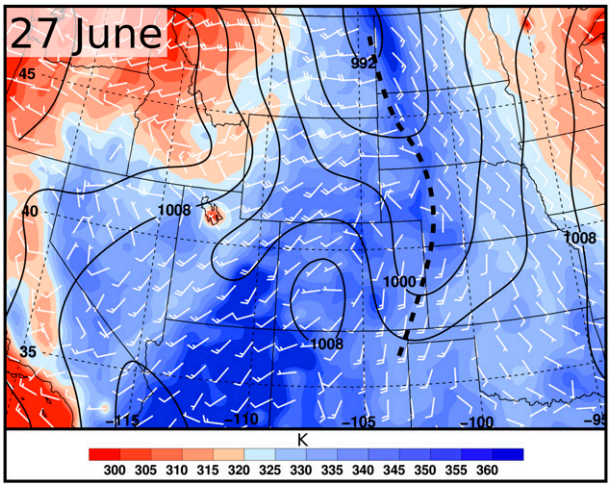

FIG. 7. Surface pressure (contours, hPa), winds, and equivalent potential temperature (color, K) at 0000 UTC 27 Jun 2012.

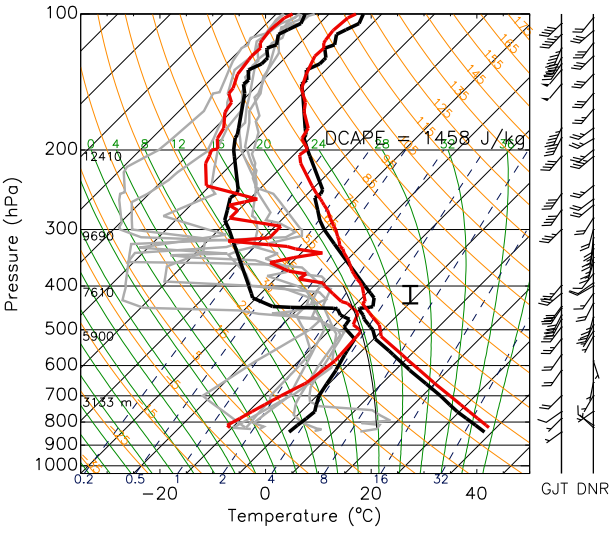

FIG. 8. Soundings from Denver (DNR, red) and Grand Junction (GJT, black), Colorado, at 0000 UTC 27 Jun 2012. Downdraft convective available potential energy (DCAPE, computed for the vertical interval denoted in the plot) for DNR is indicated. To illustrate the relatively moist conditions aloft at DNR at 0000 UTC 27 Jun 2012, dewpoint curves for DNR soundings from 0000 UTC 24 Jun to 1200 UTC 26 Jun 2012 are shown in gray.

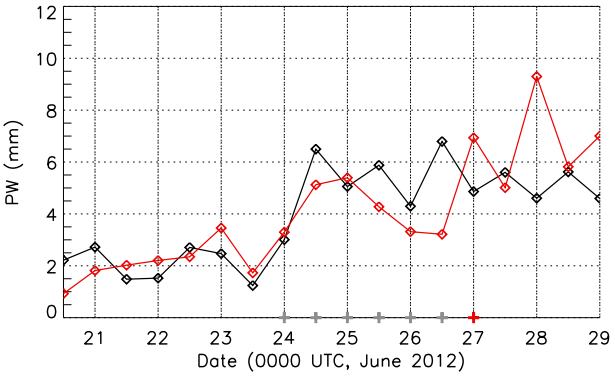

FIG. 9. Precipitable water (PW; mm) above 600 hPa in soundings from Denver (DNR, red) and Grand Junction (GJT, black) from 1200 UTC 20 Jun to 0000 UTC 29 Jun 2012. Gray pluses on abscissa refer to times for gray dewpoint curves as in Fig. 8, red plus for time for full soundings as plotted in Fig. 8. Increasing moisture aloft with time reflects increasing potential for strong downdrafts from high-based showers.

c. *Numerical simulations*

The National Center for Atmospheric Research (NCAR) Advanced Research Weather Research and Forecasting Model (ARW; Skamarock et al. 2008) was run over a domain covering most of the central two-thirds of the United States (shown in Fig. 16, later) for 27 h from 0000 UTC 26 June to 0300 UTC 27 June. The simulation used a 4-km horizontal grid spacing and 51 vertical levels on a stretched grid. Initial and lateral boundary conditions were from the 0.5° GFS model. The boundary conditions are based on GFS forecasts, so the simulation could have been run in real time (i.e., it is technically a "reforecast"). Physics packages include Morrison double-moment microphysics (Morrison et al. 2005), the Rapid Radiative Transfer Model (RRTMG; Iacono et al. 2008), and the Mellor–Yamada–Janjić (MYJ; Mellor and Yamada 1982; Janjić 2002) boundary layer scheme. Convection was treated explicitly (i.e., no cumulus parameterization was used).

4. Large-scale environmental conditions

a. *Synoptic setting*

The primary feature of the large-scale flow during this period was a strong, persistent ridge over the central United States and troughs on both the east and west coasts (Fig. 5). During the 24-h period from 0000 UTC 26 June to 0000 UTC 27 June (subtract 6 h to obtain local time), a shortwave trough moved across the Pacific Northwest in association with a slight flattening and eastward shift of the central U.S. ridge (Figs. 5a,b). Over

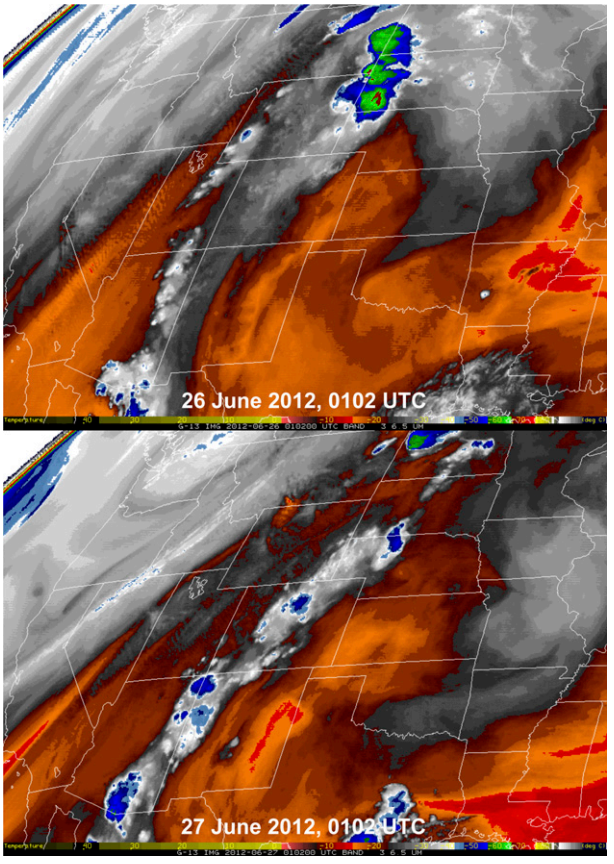

FIG. 10. *GOES-13* water vapor imagery for 0102 UTC (top) 26 and (bottom) 27 Jun 2012.

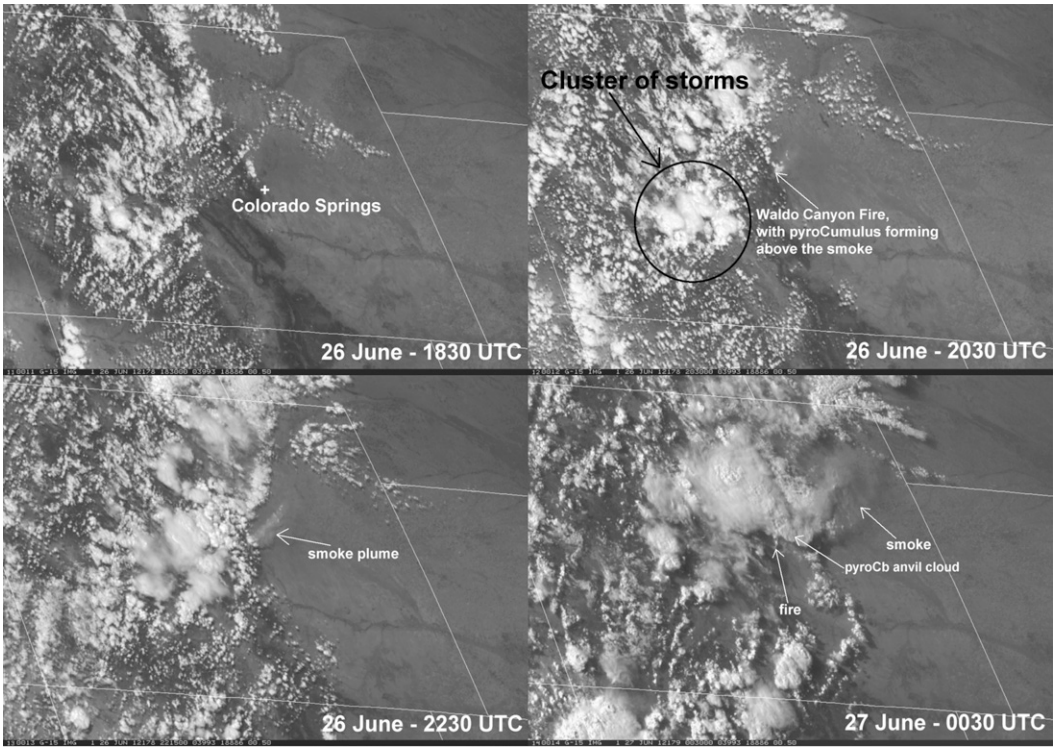

FIG. 11. *GOES-15* visible imagery at 1830, 2030, and 2230 UTC 26 Jun and 0030 UTC 27 Jun 2012. Locations of cluster of storms that generated the outflow, fire, smoke plume, and pyrocumulus are indicated.

the same period, southerly to southwesterly flow increased over the southern Intermountain West as absolute vorticity maxima approached from the west. Maps of precipitable water over a 3-day period starting at 0000 UTC 24 June (Fig. 6) reveal that this increased southerly-southwesterly flow aided the wrapping of an eastern Pacific moisture tongue around a 700-hPa anticyclone, which led to increased moisture over the Colorado–Utah region by the evening of 26 June.

On the afternoon of 26 June, a surface low pressure area extended from eastern Colorado northward to eastern Montana (Fig. 7). Over Colorado, the feature took the form of a lee trough east of the Rocky Mountains, while the extension of the low over Montana was associated with the shortwave trough moving inland from the west coast (Fig. 5b). The lee trough along the Colorado Front Range led to moderate southwesterly low-level flow across the Waldo Canyon fire area. The eastern Pacific moisture tongue in precipitable water (Fig. 6d) was reflected at the surface as a region of high surface equivalent potential temperature (>360 K) over Arizona, which was being advected toward Colorado by southwesterly flow (Fig. 7).

Soundings in the late afternoon on 26 June from Denver and Grand Junction, Colorado, representing conditions across the state, are shown in Fig. 8 (0000 UTC 27 June, heavy curves). At both stations the temperature and moisture stratification reflects nearly ideal ''microburst'' conditions, as described by Wakimoto (1985). The approximately dry adiabatic and constant specific humidity profiles from near the surface to 500 hPa (an ''inverted V'' pattern) are conducive to strong downdrafts if precipitation develops from clouds in the layer above. Downdraft convective available potential energy (DCAPE; Gilmore and Wicker 1998; Potter 2002) in the DNR sounding was exceptionally large (1458 J kg^{-1}) compared to values reported in other high-wind situations (Kuchera and Parker 2006), reinforcing the fact that the profile was conducive to strong downdrafts.

Further enhancing the downdraft potential, the atmosphere at DNR at 0000 UTC 27 June was moister aloft than on preceding days, whose dewpoint profiles are indicated in Fig. 8 (gray curves) going back to 0000 UTC 24 June. In particular, the precipitable water (PW) in the column above 600 hPa at 0000 UTC 27 June was greater than it had been at any time during the previous week, as shown in the PW time series in Fig. 9. Both DNR and GJT show a general upward trend in PW over this period. Moistening aloft is an important factor in the strength of downbursts (given a dry-adiabatic subcloud layer) since greater moisture in the cloud layer implies more precipitation production, which then yields

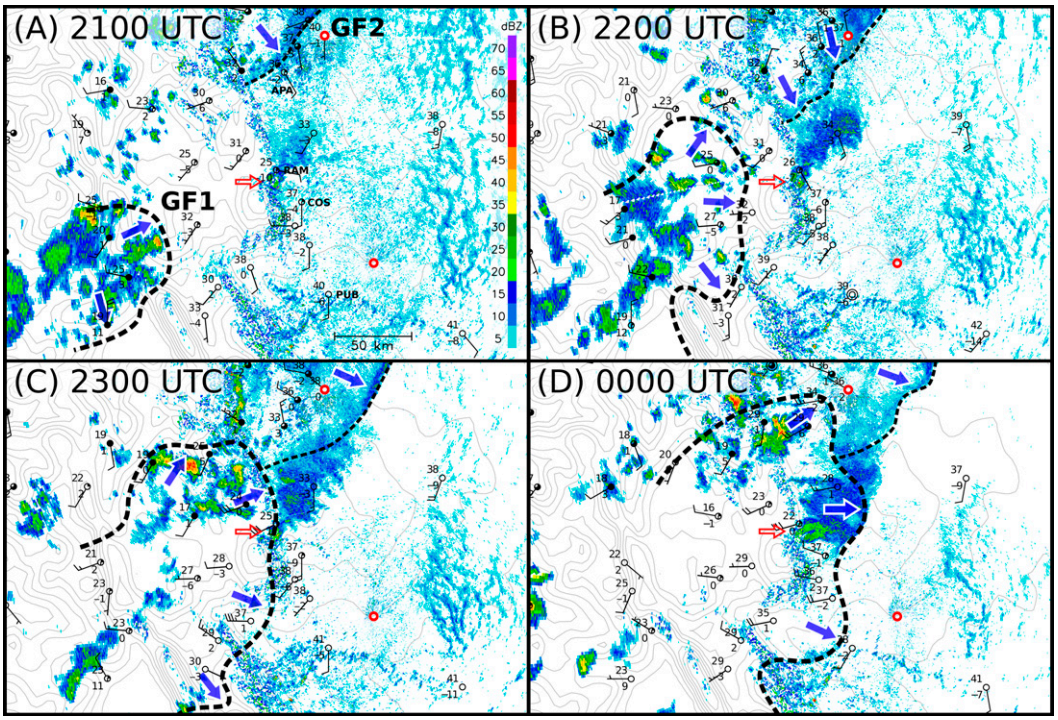

FIG. 12. Winds ($m\,s^{-1}$: one full barb = $5\,m\,s^{-1}$, one-half barb = $2.5\,m\,s^{-1}$), temperature and dewpoint (°C), and mosaic base radar reflectivity for the periods (a) 2100, (b) 2200, (c) 2300 UTC 26 Jun, and (d) 0000 UTC 27 Jun 2012. Two gust front (GF1 and GF2) positions (dashed lines) are located based on high-time-resolution data from surface stations and radar reflectivity and velocity data from Denver (FTG) and Pueblo (PUX) radars (red circles). See Fig. 4 for locations of stations. Red arrow points to Waldo Canyon fire and blue arrows indicate direction of surface flow. Locations of meteogram sites (APA, RAM, COS, and PUB) in Fig. 13 are indicated in 2100 UTC panel. Smoke plume is reflectivity maximum to the northeast of the fire location in (b) and (c), which shifts to more easterly direction at 0000 UTC in (d). Terrain interval is 200 m.

greater evaporation and stronger downdrafts (Wakimoto 1985). As will be seen, precipitating clouds developed over the region by midafternoon on 26 June with much of the precipitation evaporating before reaching the ground, an ideal situation for strong downdrafts.

b. *Satellite imagery*

A sequence of two *GOES-13* water vapor images 24 h apart in the late afternoon on 25 and 26 June (0102 UTC on 26 and 27 June, respectively) is shown in Fig. 10. A plume of moisture extended northward along the Arizona–New Mexico border into eastern Utah–western Colorado on 25 June (Fig. 10a), and then into central Colorado on 26 June (Fig. 10b). The 6.5-μm water vapor channel has maximum weighting in the 300–500-hPa layer, so the axes of the GOES water vapor plumes do not coincide exactly (are displaced eastward in this case) with the positions of the moist tongues (Figs. 6c,d). The lines of storms that developed over central Utah at 0102 UTC 26 June were linked most closely to the axis of the precipitable water maximum (Fig. 6c). Twenty-four hours later (Fig. 10b) the convection shifted to central Colorado, where it was tightly aligned along the rather narrow upper-tropospheric water vapor plume. The eastward shift of the axis of upper-level moisture is consistent with the increased PW above 600 hPa at 0000 UTC 27 June (Fig. 9).

5. Mesoanalysis of convective systems on 26 June

The convective system that eventually impacted the Waldo Canyon fire first formed over the San Juan Mountains in southwestern Colorado at midday on 26 June (Fig. 11). As this sequence of visible images shows, the convective complex (indicated by a circle at 2030 UTC) grew in size over a 6-h period and moved northeastward, passing to the northwest of Colorado Springs. As will be seen, even though the storm did not pass directly over Colorado Springs, the downdraft outflow from it had a major impact on the evolution of the fire.

As the convective system over the San Juan Mountains grew in size and moved northeastward, it produced

a pronounced convective outflow with a leading gust front (labeled GF1) at the surface by 2100 UTC (Fig. 12a). Given the "downburst type" environment within which the convection formed and the large area of the outflow, the event can be referred to as a "macroburst" by the definition of Fujita (1985). Although radar beam blockage is a problem in this part of Colorado (Maddox et al. 2002), a cluster of convective cells was clearly evident at 2100 UTC, as was another area of convection and associated gust front (GF2) to the west of Denver (northern part of analysis domain). Over the next two hours (Figs. 12a–c), GF1 expanded and moved northeastward with scattered convection at its leading edge, reaching a position at 2300 UTC where it just began to impact the Waldo Canyon fire. GF2, on the other hand, moved southeastward, although it was still well north of the Colorado Springs area. At 0000 UTC 27 June (Fig. 12d), GF1 had passed the fire and a shift in direction and expansion of the smoke plume more to the east can be seen. The estimated average speed of the gust front GF1 over the 3-h period is 15 m s^{-1}. GF2 remained north of the Waldo Canyon fire at 0000 UTC.

Meteograms for four sites, arranged from north to south along the Colorado Front Range are shown in Fig. 13. Figure 13b shows the passage of GF1 at the Air Force Academy mesonet site atop Rampart Ridge (location shown in Figs. 2 and 4) just before 2300 UTC, accompanied by a temperature drop of ~5°C, a relative humidity increase of ~15%, and wind gusts to 26 m s^{-1}. In addition, at Manchester, a RAWS station 40 km northwest of Colorado Springs (Fig. 4), a sustained wind of 37 mph (17 m s^{-1}) from the west-southwest was reported at 2300 UTC, with a gust to 59 mph (26 m s^{-1}) during the previous hour (precise time not known). Centennial Airport (APA) and Colorado Springs (COS) (Figs. 13a,c) indicate the GF1 passage shortly thereafter, namely, a sudden shift to strong westerlies (with a gust to 23 m s^{-1} at APA) between 2300 UTC 26 June and 0000 UTC 27 June. At APA (Fig. 13a), GF1 passage was preceded by GF2 passage between 2100 and 2200 UTC, although GF2 never reached COS (Fig. 13c) prior to GF1's arrival. However, a new outflow did appear to reach COS between 0100 and 0200 UTC after the passage of GF1 with a shift to north-northwesterly flow. Whether this wind shift was associated with GF2 or new convection that formed 20–30 km north of the fire at 0000 UTC (Fig. 12) is unclear. GF1 arrived at Pueblo (PUB), Colorado, around 0030 UTC. At the time of the gust front passage, there were media reports of winds up to 65 mph (29 m s^{-1}), but those reports could not be confirmed. Winds of the magnitude reported at several of the sites would clearly have a major impact on the progression of the fire.

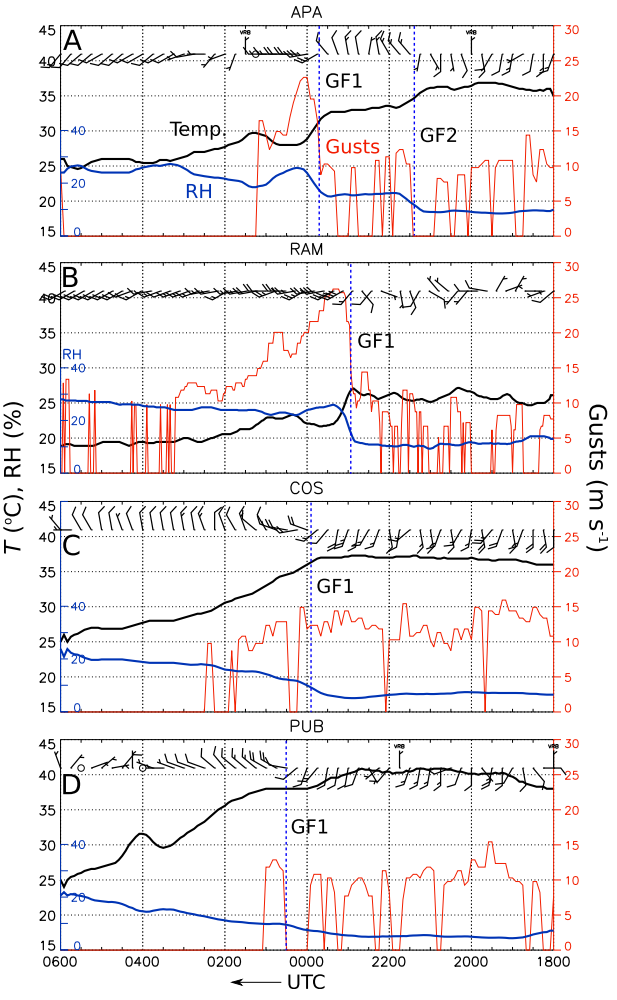

FIG. 13. Meteograms of winds (plotting as in Fig. 12), temperature and dewpoint (°C), and peak wind gusts (m s^{-1}) at (a) Centennia (APA), (b) Rampart Ridge (RAM), (c) Colorado Springs (COS), and (d) Pueblo (PUB) from 1800 UTC 26 Jun to 0600 UTC 27 Jun 2012. See Fig. 4 for station locations. Vertical lines mark times of GF1 and GF2 passage. Data frequency at RAM is 2 min and 5 min for the other sites.

6. Radar and supporting observations of the gust front and fire

A sequence of radar reflectivity and radial velocity images from the Pueblo radar at 1-h intervals from 2300 UTC 26 June to 0100 UTC 27 June is shown in Fig. 14. The reflectivity image at 2300 UTC (Fig. 14a) shows the smoke plume[4] moving off to the northeast carried by

[4] The radar reflectivities over the mountainous area to the west are due to precipitation systems, while those associated with the fire are principally due to ash and soot. However, by 0000 UTC, pyrocumulonimbus had formed (Lang et al. 2014), so some of the radar reflectivity by that time was due to the presence of hydrometeors.

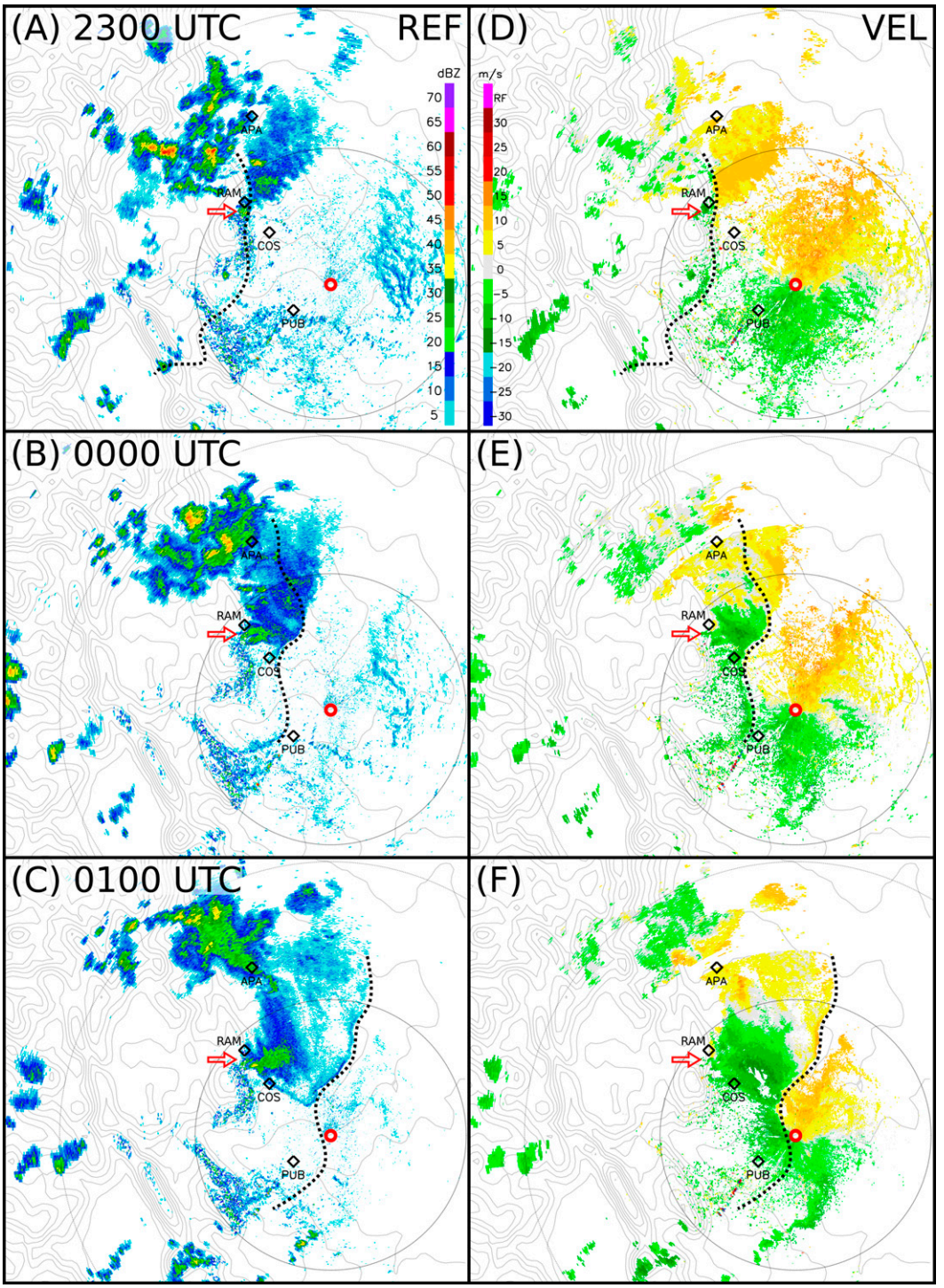

FIG. 14. Sequence of (a)–(c) base radar reflectivity and (d)–(f) radial velocity images from Pueblo, Colorado, WSR-88D (red circle) from 2300 UTC 26 Jun to 0100 UTC 27 Jun 2012. Red arrow denotes location of Waldo Canyon fire. Gust front positions are indicated by dotted line. Range rings are at 100-km intervals and terrain interval is 200 m.

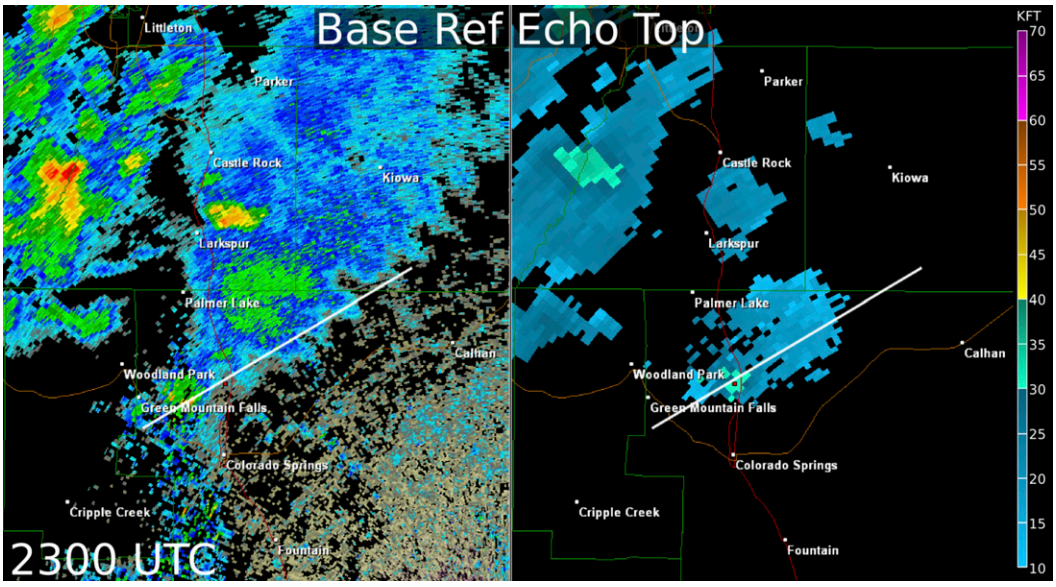

FIG. 15. (left) Radar reflectivity plot (same scale as in Fig. 12) centered over fire plume and (right) radar echo tops (scale on right) at 2300 UTC 26 Jun 2012. White line denotes location of transect in Fig. 16.

the southwesterly flow aloft. By 0000 UTC (Fig. 14b), the gust front had moved through the fire area, causing a broadening and eastward shift of the smoke plume. An hour later, at 0100 UTC (Fig. 14c), further expansion of the smoke plume can be seen along with a continuing eastward shift as the gust front, marked by a thin reflectivity line, moved out onto the plains.

The passage of the gust front can be better seen in the Pueblo radial velocity images (Figs. 14d–f). A wind-shift line separating southwesterly (orange/yellow colors) from westerly or northwesterly (green colors) flow moved through the location of the fire at 2300 UTC (Fig. 14d) and then eastward as the smoke plume expanded. The speed of the wind-shift line in the fire plume determined from an animation of the velocity images was 16–17 m s^{-1}, which is close to the estimated speed of the gust front based on the surface mesoanalyses. (See animations of radar reflectivity and radial velocity in the online supplemental material.) The peak inbound radial velocities in the plume at 0000 UTC (Fig. 14e) exceeded 15 m s^{-1} behind the gust-front boundary, which was well in excess of the lower-tropospheric winds at Denver at 0000 UTC (Fig. 8) and is indicative of convective outflow dynamics. Continued eastward progression of the gust front is also seen in the radial velocity field at 0100 UTC (Fig. 14f).

A zoomed-in radar reflectivity image centered on the fire at 2300 UTC is shown in Fig. 15, along with radar echo-top information. The fire plume extends off to the northeast while convective cells are scattered throughout the northwestern portion of the domain. Highest echo tops seen in the figure are near 11 km (~35 000 ft), although Lang et al. (2014) indicate tops to 13 km and higher around this time.

A rapid increase in the vertical extent of the radar reflectivity column is apparent from 2200 to 2230 UTC (Figs. 16a,b), somewhat before the time of the wind shift inferred from station data. This intensification is likely related to diurnal heating cycle, the record-high temperatures, and the deep convective boundary layer. Increased reflectivities aloft continue beyond to 2300 and 2330 UTC (Figs. 16c,d). This intensification of the fire was manifested in intracloud lightning activity reported by Lang et al. (2014), where they noted a first increase at 2310 UTC and a second stronger burst at 2345 UTC. Lang et al. (2014) point out that the only lightning activity with the Waldo Canyon fire occurred at the time of the passage of the gust front on the afternoon of 26 June, suggesting that the arrival of the convective outflow was an important contributor to the intensification of the fire as inferred from the pyrocumulonimbus activity.

The radial velocity field from the Pueblo radar varied little between 2200 and 2300 UTC (Figs. 16e–g), but a marked change is seen between 2300 and 2330 UTC (Figs. 16g,h). During this period, there is clear evidence of the gust front moving past the fire out onto the plains from a pronounced increase in low-level radar reflectivity and outbound (southerly) flow switching to inbound (westerly) flow in the lowest 2–3 km, the approximate depth of the convective outflow. As the gust front surged eastward during this later period, there is

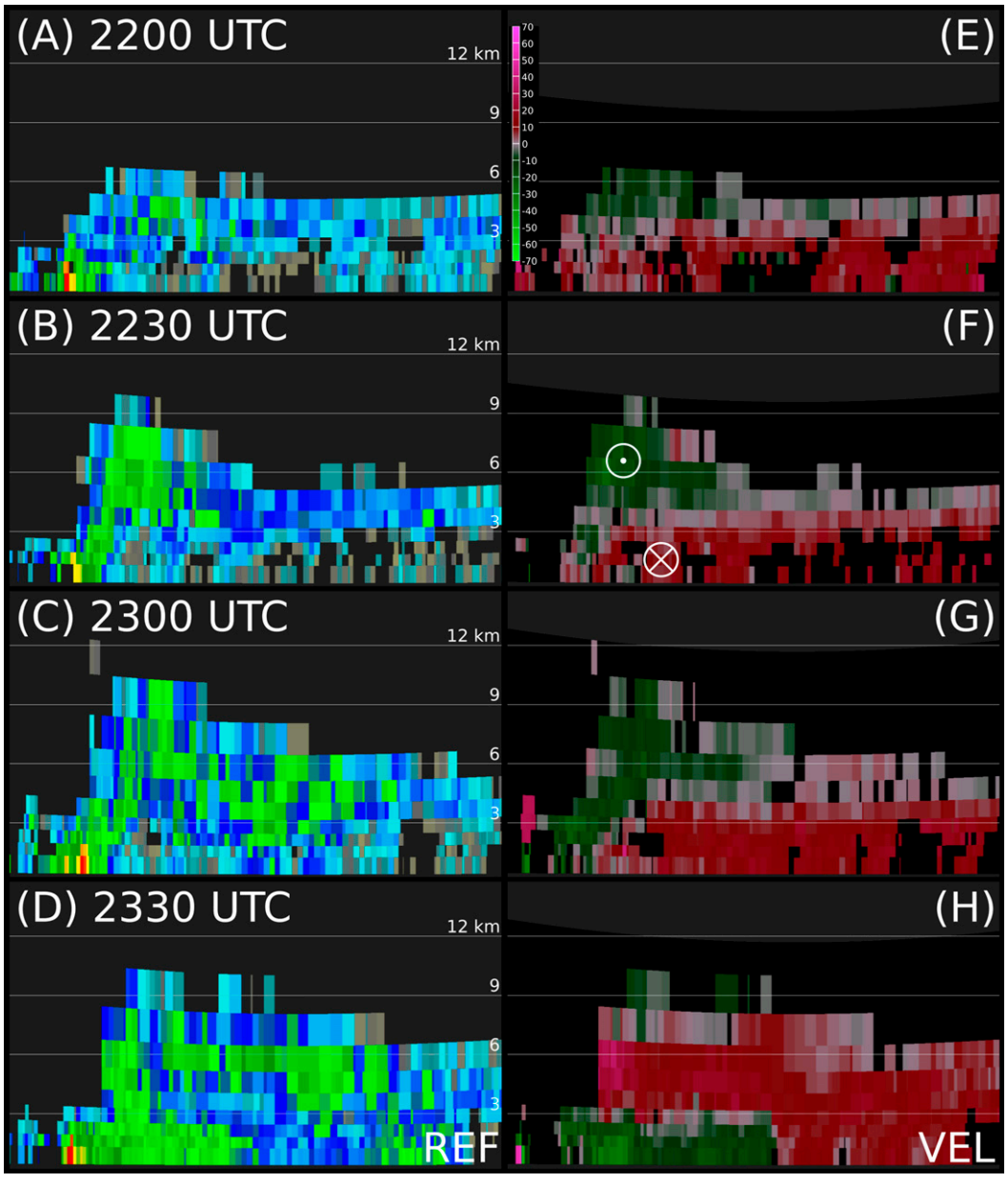

FIG. 16. Vertical cross sections of (a)–(d) radar reflectivity (same scale as in Fig. 15) and (e)–(h) radial velocity ($m\,s^{-1}$) based on Pueblo (PUX) radar from 2200 to 2330 UTC 26 Jun 2012. Heights are distances above ground level. Circled dot (crisscross) denotes flow into (out of) the page.

a suggestion that the southerly (outbound) velocities are scoured and lifted upward over the outflow itself (Figs. 16g,h).

The effect of the convective outflow on the fire's ash plume is further depicted in a 3D perspective over a 37-min period from 2301 to 2338 UTC in Fig. 17. Ashes and other debris from the fire are the source of the radar reflectivity and can be seen to quickly spread eastward in the lowest 3 km undercutting the plume aloft. The plume aloft also comprised ice particles, which are necessary to produce the observed lightning (Lang et al. 2014). It is this rapid eastward advance of the low-level gust front that quickly spread the fire into the western suburbs of Colorado Springs.

The passage of the gust front through the fire area is further corroborated by the 2-min observations from the Air Force Academy mesonet. Regional plots of mesonet data at times closely corresponding to the 3D images in

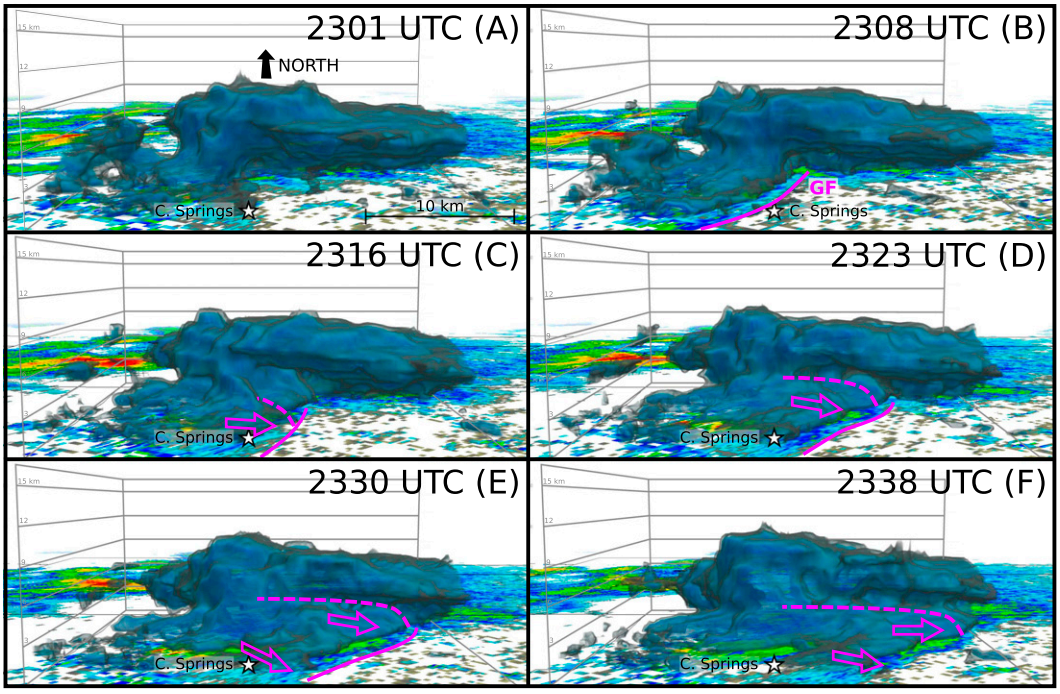

FIG. 17. Three-dimensional depictions of radar reflectivity at ~7-min intervals from (a)–(f) 2301 to 2338 UTC 26 Jun 2012 from Pueblo WSR-88D. Approximate position of low-level gust-front boundary (GF) is indicated. Two shells of reflectivity are highlighted: −2 to +2 dBZ for gray outer shell and 7–12 dBZ for blue shell.

Fig. 17 are presented in Fig. 18, along with the analyzed location of the gust front. The gust front position, including a forward bulge in it that develops after ~2315 UTC, and its movement through the area as determined from the mesonet data correspond well to the same features depicted in the other analyses (Figs. 12, 14, and 17). Cooling, increased relative humidity, and stronger and gusty winds are observed following the passage of the outflow boundary. The speed of the gust front at the latitude of the northern fringe of the burn area is ~17 m s^{-1}, which is in good agreement with the speed estimated from the radar and other surface analyses.

7. Simulated convection and associated gust fronts

The ARW was run for 27 h starting at 0000 UTC 26 June and ending at 0300 UTC 27 June. The 27-h total precipitation for the simulation is shown in Fig. 19. An elongated zone of generally light precipitation is forecast in a band along the moisture plume (Fig. 9) extending from Arizona into the northern plains.

Shown in Figs. 20a–d are a sequence of mesoanalyses from the simulation for this case for the period 2000–2300 UTC. For comparison purposes, these analyses of simulated radar reflectivity, surface winds, and surface potential temperature have been constructed over the same domain as the observed outflows in Fig. 12, though the timing for each panel is one hour earlier. The simulated storms that produced the precipitation across Colorado were mainly grouped into organized convective complexes with associated extensive surface downdraft outflows. In agreement with observations, the model produces two organized outflows and associated gust fronts (GF1 and GF2) that move from the mountains onto the eastern plains of Colorado. The largest discrepancy is that the timing of the gust front passage at the Waldo Canyon fire is approximately two hours too early (cf. Figs. 12 and 20).

Simulated vertical cross sections showing the passage of GF1 down the slopes of the Rocky Mountain terrain are presented in Figs. 21a–d for the period 1900–2200 UTC. Once again, the timing of the passage of GF1 is approximately two hours earlier in the model than observed. As the gust front moves over the various ridges to the west of the fire, both the winds and potential temperature structures indicate the occurrence of hydraulic jumps on the downwind sides of individual barriers (Smith 1989). Such phenomena typically occur during the cold season in association with downslope windstorms (Durran 1990), whose dynamics are explained in terms of shallow water flowing over an obstacle (Long 1954). However, the passage of a cold pool

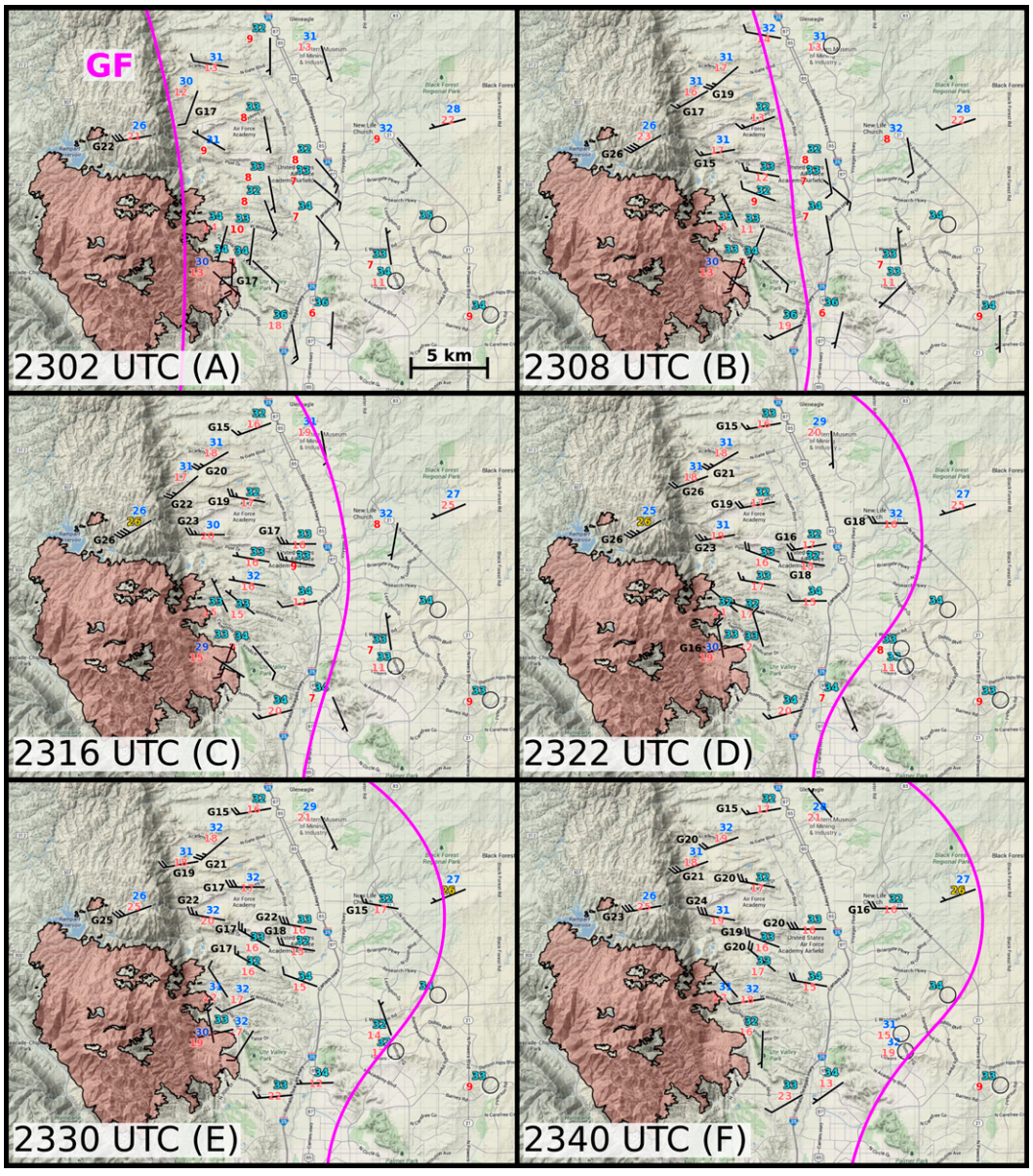

FIG. 18. Plots of Air Force Academy mesonet and other nearby surface data (a)–(f) from 2302 to 2340 UTC 26 Jun 2012, closely corresponding to times of radar depictions shown in Fig. 17. Analyzed position of gust front (GF) is indicated. Temperature (°C) is in blue (values ≥32.0°C light blue, <32.0°C dark blue); relative humidity (RH in %, plotted below the temperature) is in dark red for RH < 10%, light red for 11% < RH < 25%, and yellow for RH > 25%; wind speeds are in m s^{-1} (one full barb = 5 m s^{-1}, one-half barb = 2.5 m s^{-1}); and wind gusts ≥15 m s^{-1} are indicated. For reference, final fire perimeter is denoted.

associated with a convective outflow over mountain barriers could well exhibit similar dynamics. The existence of a hydraulic jump in the vicinity of the fire could have not only intensified the downslope winds, but also lengthened the duration of the high winds.

Early on (Figs. 21a–c), the gust front has a relatively strong temperature gradient associated with it (1900–2100 UTC), but by the time it has passed the fire (2200 UTC; Fig. 21d), the temperature gradient has weakened considerably. This weakening is likely related to the fact that the convection driving the outflow has mostly died out by this time and the cold pool has now moved far from its source. When the simulated cold pool reaches the fire (Fig. 21c), its depth is approximately 2 km, which is roughly consistent with the observations shown in Fig. 16.

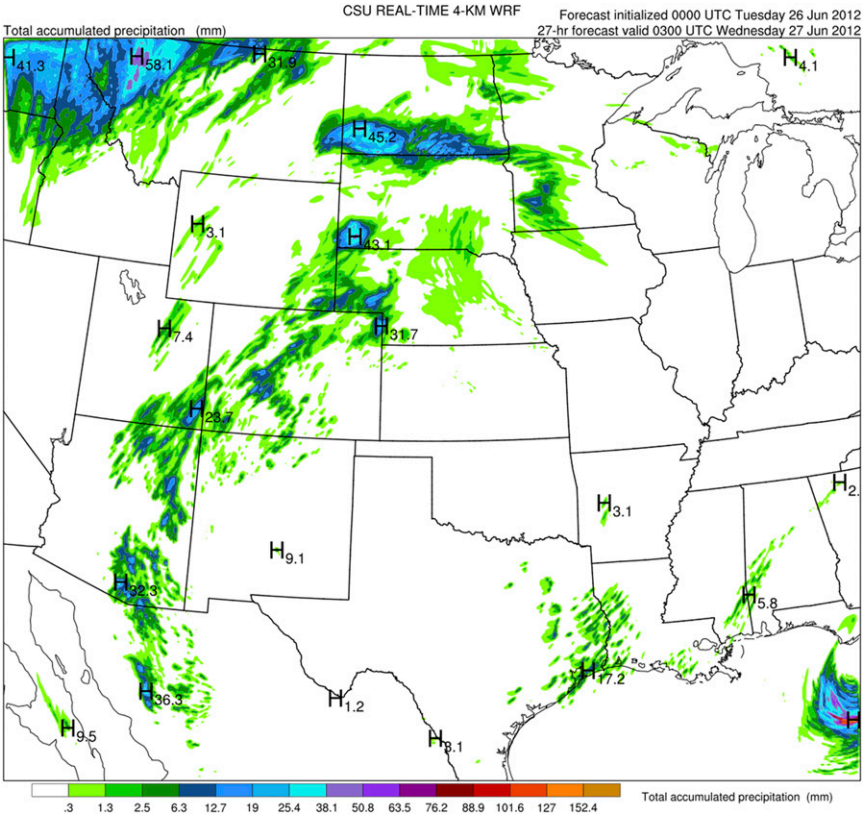

FIG. 19. The 27-h total precipitation (mm) for ARW forecast starting at 0000 UTC 26 Jun 2012.

(Animations of the simulations can be found in the online supplemental material.)

8. Summary and conclusions

The meteorological conditions accompanying the rapid spread of the catastrophic Waldo Canyon fire on 26 June 2012 in the Colorado Springs area have been investigated. The fire occurred following one of the driest and warmest winter and spring periods in recorded history over the Intermountain West. In terms of economic loss, the Waldo Canyon fire was the most destructive wildland fire on record in Colorado.

On the afternoon of 26 June, the Waldo fire rapidly intensified and quickly advanced into a densely populated neighborhood in the northwest part Colorado Springs, destroying nearly 350 homes. Mesometeorological analyses combined with reports from surface observers show that rapidly changing weather conditions played a key role in the sudden advance of the fire during the afternoon. Based on observations from a variety of surface stations over Colorado, as well as numerical simulations, evidence is presented to show that the rapid spread and further intensification of the fire was timed with the afternoon passage of a strong gust front across the region. The gust front had its origins within a thunderstorm complex that formed during midday over the San Juan Mountains of southwestern Colorado.

The synoptic-scale setting on 26 June featured a strong upper-level high over the central United States with relatively weak southwesterly flow over Colorado. On the preceding day, a tongue of moist air emanating from northwestern Mexico streamed into southern Utah leading to afternoon thunderstorms in that state. The moisture plume then shifted eastward to Colorado on 26 June and along with very dry conditions in the lower troposphere, created ideal conditions for high-based thunderstorms accompanied by strong microbursts. Indeed, the thunderstorms that first formed at midday over southwestern Colorado, upon moving to the south-central part of the state, produced a large, organized convective downdraft outflow (a macroburst) that moved eastward at about 15 $m\,s^{-1}$, arriving at the location of the Waldo Canyon fire at about 2300 UTC (1700 LT). Timed with the passage of the gust front

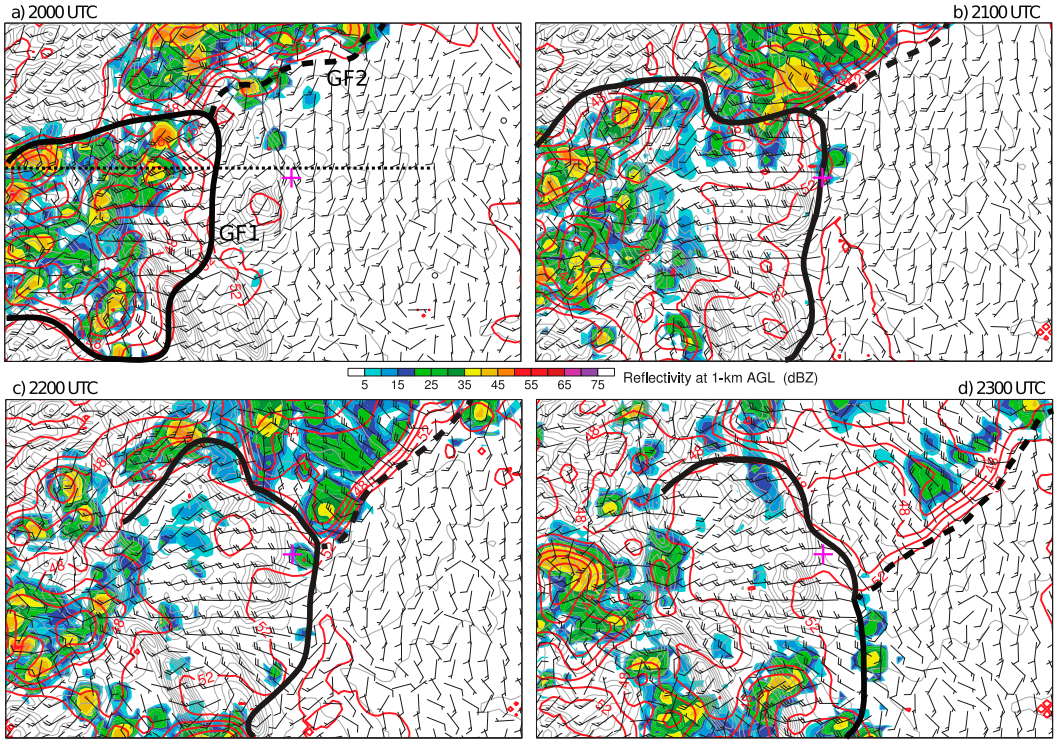

FIG. 20. Simulated radar reflectivity at 1-km AGL and surface winds, and potential temperature (2°C interval) from (a)–(d) 2000 to 2300 UTC 26 Jun 2012. Terrain interval is 200 m. Two gust fronts (GF1 and GF2) are indicated. Plus denotes location of Waldo Canyon fire. Dotted line in (a) indicates position of vertical cross section in Fig. 21.

passage was an intensification of the fire as evidenced by the formation of pyrocumulonimbus (Fig. 3) and a sudden onset of lightning activity (Lang et al. 2014). Simultaneously, the strong westerly flow accompanying the gust front pushed the fire downhill into the residential area on the west side of Colorado Springs. A secondary cold pool and gust front occurred to the north of Colorado Springs, but it did not reach the location of the fire.

Numerical simulations of the event using a 4-km version of the ARW starting with initial conditions one day earlier produced a realistic representation of the sequence of events on this day. The model successfully simulated the gust front that passed through the fire as well as the second outflow to north, although the timing was approximately two hours too early. The overall dimensions and structure of the outflow systems agreed very well with the observations. The modeled vertical structure of the gust front affecting the fire showed it to be a ~2–3-km-deep cold pool with a temperature contrast at its leading edge weakening with time as it moved eastward away from the convective source region. As the cold pool passed over ridges along the sloped terrain on the east slopes of the Rocky Mountains, it produced hydraulic jumps to the lee of individual barriers, which could have played a role in accelerating the spread of the fire. While the organized convective complexes and overall positions and shapes of both GF1 and GF2 are well simulated, the utility of such forecasts a day in advance for specific decision making related to the fire (e.g., occurrence and timing of gust front passages) is problematic given the multifaceted and complex interactions that can occur in convective environments over complex terrain. However, the model was able to capture changes in the synoptic environment that made conditions on 26 June more conducive to strong downbursts and convective outflows from high-based thunderstorms over Colorado, which eventually spread out over a large area and impacted the fire.

Acknowledgments. The IMETs gratefully acknowledge the assistance of the NWS Pueblo Weather Forecast Office for providing critical weather information and support throughout the fire. Thorough reviews by three referees led to substantial improvements in the paper. We thank the National Weather Service Forecast Office Pueblo for supplying the original version of Fig. 2. The office is acknowledged for providing critical forecasting support for the fire. We also thank Tim Lang for his helpful comments on the lightning behavior of the

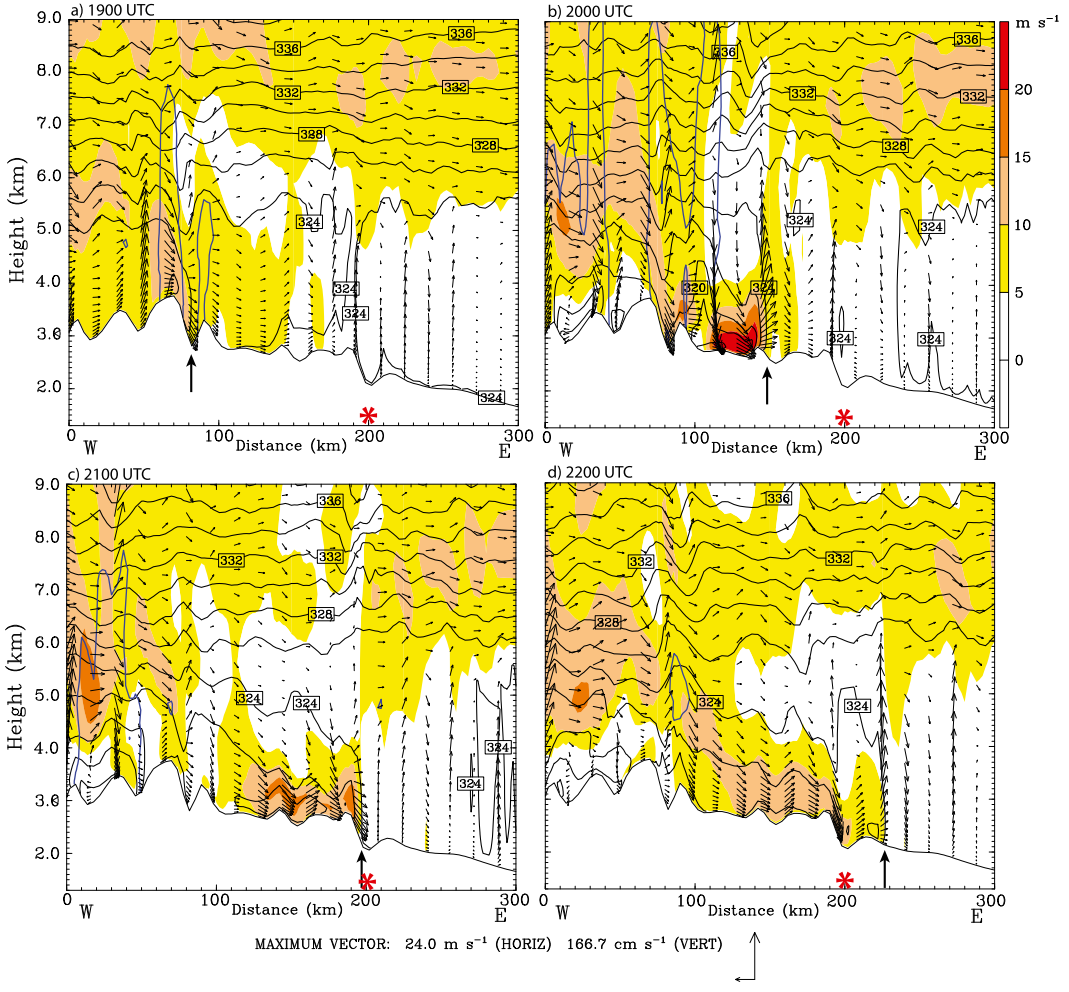

FIG. 21. East–west cross section (see Fig. 20 for location) of simulated winds (vectors, with magnitude in m s^{-1} in color) and potential temperature (K) from (a)–(d) 1900 to 2200 UTC 26 Jun 2012. Location of precipitation is indicated by 20-dBZ simulated reflectivity contours (blue). Leading edge of gust front is marked by arrow and approximate longitude of the leading edge of the fire by asterisk.

fire. This research has been partially supported by the National Science Foundation under Grant AGS-1059899. The views, opinions, and findings in this report are those of the authors, and should not be construed as an official NOAA and or U.S. government position, policy, or decision.

REFERENCES

Corfidi, S. F., S. J. Corfidi, and D. M. Schultz, 2008: Elevated convection and castellanus: Ambiguities, significance, and questions. *Wea. Forecasting,* **23,** 1280–1303, doi:10.1175/2008WAF2222118.1.

Diaz, H. F., and T. W. Swetnam, 2013: The wildfires of 1910: Climatology of an extreme early twentieth-century event and comparison with more recent events. *Bull. Amer. Meteor. Soc.,* **94,** 1361–1370, doi:10.1175/BAMS-D-12-00150.1.

Durran, D. R., 1990: Mountain waves and downslope winds. *Atmospheric Processes over Complex Terrain, Meteor. Monogr.,* No. 45, Amer. Meteor. Soc., 59–81.

Engel, C. B., T. P. Lane, M. J. Reeder, and M. Rezny, 2013: The meteorology of Black Saturday. *Quart. J. Roy. Meteor. Soc.,* **139,** 585–599, doi:10.1002/qj.1986.

Fromm, M., D. T. Lindsey, R. Servranckx, G. Yue, T. Trickl, R. Sica, P. Doucet, and S. Godin-Beekman, 2010: The untold story of pyrocumulonimbus. *Bull. Amer. Meteor. Soc.,* **91,** 1193–1209, doi:10.1175/2010BAMS3004.1.

Fujita, T. T., 1985: *The Downburst: Microburst and Macroburst.* University of Chicago, 122 pp.

Gilmore, M. S., and L. J. Wicker, 1998: The influence of midtropospheric dryness on supercell morphology and evolution. *Mon. Wea. Rev.,* **126,** 943–958, doi:10.1175/1520-0493(1998)126<0943:TIOMDO>2.0.CO;2.

Horel, J., and Coauthors, 2002: Mesowest: Cooperative mesonets in the western United States. *Bull. Amer. Meteor. Soc.,* **83,** 211–225, doi:10.1175/1520-0477(2002)083<0211:MCMITW>2.3.CO;2.

Iacono, M. J., J. S. Delamere, E. J. Mlawer, M. W. Shephard, S. A. Clough, and W. D. Collins, 2008: Radiative forcing by long-lived greenhouse gases: Calculations with the AER radiative transfer models. *J. Geophys. Res.,* **113,** D13103, doi:10.1029/2008JD009944.

Janjić, L., 2002: Nonsingular implementation of the Mellor–Yamada level 2.5 scheme in the NCEP Meso model. NCEP Office Note 437, National Centers for Environmental Prediction, 61 pp.

Johnson, R. H., R. S. Schumacher, and D. T. Lindsey, 2013: Weather impacts on the June 2012 Waldo Canyon Fire disaster. *Impacts: Weather 2012,* Austin, TX, Amer. Meteor. Soc., 3.4. [Available online at https://ams.confex.com/ams/93Annual/webprogram/Paper224455.html.]

Kuchera, E. L., and M. D. Parker, 2006: Severe convective wind environments. *Wea. Forecasting,* **21,** 595–612, doi:10.1175/WAF931.1.

Lang, T. J., S. A. Rutledge, B. Dolan, P. Krehbiel, W. Rison, and D. T. Lindsey, 2014: Lightning in wildfire smoke plumes observed in Colorado during summer 2012. *Mon. Wea. Rev.,* **142,** 489–507, doi:10.1175/MWR-D-13-00184.1.

Long, R. R., 1954: Some aspects of the flow of stratified fluids. II. Experiments with a two fluid system. *Tellus,* **6,** 97–115, doi:10.1111/j.2153-3490.1954.tb01100.x.

Maddox, R. A., J. Zhang, J. J. Gourley, and K. W. Howard, 2002: Weather radar coverage over the contiguous United States. *Wea. Forecasting,* **17,** 927–934, doi:10.1175/1520-0434(2002)017<0927:WRCOTC>2.0.CO;2.

Meister, M., 2013: The Waldo Canyon Fire: Communication successes and challenges as the station scientist. *Impacts: Weather 2012,* Austin, TX, Amer. Meteor. Soc., 3.6. [Available online at https://ams.confex.com/ams/93Annual/webprogram/Paper224513.html.]

Mellor, G. L., and T. Yamada, 1982: Development of a turbulence closure model for geophysical fluid problems. *Rev. Geophys.,* **20,** 851–875, doi:10.1029/RG020i004p00851.

Morrison, H., J. A. Curry, and V. I. Khvorostyanov, 2005: A new double-moment microphysics scheme for application in cloud and climate models. Part I: Description. *J. Atmos. Sci.,* **62,** 1665–1677, doi:10.1175/JAS3446.1.

Myrick, D., and J. Horel, 2008: Sensitivity of surface analyses over the western United States to RAWS observations. *Wea. Forecasting,* **23,** 145–158, doi:10.1175/2007WAF2006074.1.

Potter, B. E., 2002: A dynamics based view of atmosphere-fire interactions. *Int. J. Wildland Fire,* **11,** 247–255, doi:10.1071/WF02008.

——, 2012: Atmospheric interactions with wildland fire behavior—II. Plume and vortex dynamics. *Int. J. Wildland Fire,* **21,** 802–817, doi:10.1071/WF11129.

Ruthford, J. E., and L. Kriederman, 2013: Weather factors influencing the behavior of the Waldo Canyon Fire. *Abstracts, 38th Annual Meeting,* North Charleston, NC, National Weather Association, P1.43. [Available online at http://www.nwas.org/meetings/abstracts/display.php?id=1730.]

Skamarock, W. C., and Coauthors, 2008: A description of the Advanced Research WRF version 3. NCAR Tech. Note NCAR/TN-475+STR, 113 pp. [Available online at http://www.mmm.ucar.edu/wrf/users/docs/arw_v3_bw.pdf.]

Smith, R. B., 1989: Hydrostatic air-flow over mountains. *Advances in Geophysics,* Vol. 31, Academic Press, 1–41, doi:10.1016/S0065-2687(08)60052-7.

Stark, J., 2013: NWS decision support services before, during and AFTER the Waldo Canyon wildfire. *Impacts: Weather 2012,* Austin, TX, Amer. Meteor. Soc., 3.5. [Available online at https://ams.confex.com/ams/93Annual/webprogram/Paper224942.html.]

Steenburgh, W. J., C. R. Neuman, G. L. West, and L. F. Bosart, 2009: Discrete frontal propagation over the Sierra–Cascade Mountains and Intermountain West. *Mon. Wea. Rev.,* **137,** 2000–2020, doi:10.1175/2008MWR2811.1.

Viegas, D. X., and A. Simeoni, 2011: Eruptive behavior of forest fires. *Fire Technol.,* **47,** 303–320, doi:10.1007/s10694-010-0193-6.

Wakimoto, R. M., 1985: Forecasting dry microburst activity over the high plains. *Mon. Wea. Rev.,* **113,** 1131–1143, doi:10.1175/1520-0493(1985)113<1131:FDMAOT>2.0.CO;2.